Temperature dependence of pressure sensitive flow in bulk metallic glass composites

Priyanka Saini[1], Yakai Zhao[2,3], Biao Li[4], Long Zhang[4,*], U. Ramamurty[2,3], R.L. Narayan[1,*]

[1]*Department of Materials Science and Engineering, Indian Institute of Technology, Delhi 110016, India*
[2]*School of Mechanical and Aerospace Engineering, Nanyang Technological University, Singapore 639798, Republic of Singapore*
[3]*Institute of Materials Research and Engineering (IMRE), Agency for Science, Technology and Research (A*STAR), 2 Fusionopolis Way, Innovis #08-03, Singapore 138634, Republic of Singapore*
[4]*Shi-changxu Innovation Center for Advanced Materials, Institute of Metal Research, Chinese Academy of Sciences, Shenyang 110016, China*

*Corresponding author; email: R.L. Narayan (rlnarayan@iitd.ac.in), Long Zhang (zhanglong@imr.ac.cn)

Abstract

The constraint factor, *C*, defined as hardness, *H*, to the yield strength, σ_y, ratio, is an indirect measure of the pressure sensitivity in materials. Previous investigations determined that while *C* is less than 3 for crystalline materials, and remains invariant with change in temperature, it is greater than 3 for bulk metallic glasses (BMGs) and increases with increasing temperature, below their glass transition temperature, T_g. In this study, the variations in *C* for two BMG composites (BMGCs), which have an amorphous matrix and *in situ* precipitated crystalline β-Ti dendrites, which in one case transforms under stress to α”-Ti and deforms by slip in the other, as a function of temperature are examined and compared with that of a BMG. For this purpose, instrumented indentation tests, with a Berkovich tip, and uniaxial compression tests were performed to measure the *H* and σ_y, respectively, on all alloys and their constituents at temperatures in the range of 0.48 and $0.75T_g$. σ_y and *H* of the BMGC with transforming dendrites (BMGC-T) increases and remains invariant with increasing temperature, respectively. Alternately, in BMG and the BMGC with non-transforming dendrites (BMGC-NT), the same properties decrease with increasing temperature. BMGC-T has the highest *C* of ~4.93 whereas that of BMGC-NT and BMG are ~3.72 and ~3.28, respectively, at $0.48T_g$. With increasing temperature, *C* of the BMG and BMGC–NT increases with temperature, but that of the BMGC-T decreases. The values of *C* and their variations as a function of temperature were explained by studying the variation of pressure sensitivity of the amorphous phase and concluding that the plastic flow in BMGCs under constrained conditions, such as indentation, is controlled by the flow resistance of the amorphous matrix whereas that in uniaxial compression, which is only partially constrained, is controlled by plasticity in both the dendrites and matrix.

Keywords: Bulk metallic glass composites; Hardness; Pressure sensitivity; Martensitic transformation

1. Introduction

In bulk metallic glasses (BMGs), macroscopic plasticity at temperatures of deformation well below the glass transition temperature, T_g, is mediated by the shear bands [1–6]. Since monolithic BMGs do not have a 'microstructure', which otherwise would resist shear band propagation, they propagate unhindered. This, in turn, leads to the fracture of BMG immediately after yielding in uniaxial tension [5,7,8]. One way to impart some post-yield global plasticity, i.e., ductility, to BMGs is to adopt the composite approach [9–26]. Of the several well-documented efforts to tailor the BMG composites (BMGCs) [13,15,16,22,27–31], those, which form a crystalline β-Ti phase inside the amorphous matrix upon solidification, are particularly promising. The size, volume fraction, and metastability of the β-Ti phase in them can be tailored to obtain the desired combination of mechanical properties in them [13,14,28,30,32]. In this study, we examine the pressure sensitivity of plastic deformation in these composites.

Unlike crystalline metals and alloys in which plastic deformation is almost-exclusively a function of the deviatoric part of the stress tensor, plasticity in amorphous materials such as BMGs and glassy polymers is pressure sensitive, i.e., the hydrostatic stress also plays a role in the flow behaviour [33–37]. Typically, pressure sensitivity results in an elevation in the flow stress of the material when hydrostatic compression is superposed on the shear stresses. Indentation, because of the prevalence of large hydrostatic stresses underneath the indenter, is a convenient method to explore the pressure sensitivity. The constraint factor, C, is determined from the ratio of the hardness, H, to the yield strength in uniaxial compression, σ_y [37]. Even in pressure-insensitive solids like crystalline metals, C is larger than 1. This is because of the constraint imposed by the surrounding matrix on the plastic flow of the material that is directly underneath the indenter tip. Based on the modified expanding cavity model developed by

Narasimhan [38], Patnaik et al. [39] concluded that the pressure-sensitive plastic flow in BMGs leads to significantly higher constraint factors than that in crystalline metals during indentation. This is attributed to the fact that the material underneath the indenter yields under the influence of the hydrostatic stresses that are exerted by the surrounding elastic cavity [33–37]. While *C* is sensitive to the geometry of the indenter, it is generally in the range of 3-4.5 for amorphous alloys [33–37] and between 1 and 3 for crystalline alloys [40,41].

On this basis, one would expect that BMGCs will have an intermediate value of *C* as they contain both the amorphous and crystalline phase. However, Narayan et al. [42] noted that *C* of β-Ti reinforced BMGCs is higher than even that of BMGs. This was attributed to the greater constraint imposed by the pressure sensitive amorphous matrix on the composite flow characteristics than that by its crystalline dendrites during indentation. However, they only considered BMGCs, which have dendrites that undergo dislocation slip and hence exhibit negligible pressure sensitivity. Zhang et al. [13,27,43] have recently developed BMGCs in which the β-Ti dendrites undergo yielding via stress induced martensitic transformation (SIMT) to α”-Ti, similar to that in β-Ti alloys [44,45]. Given that such phase transformations involve some volume change, it is worth investigating if the volumetric strain developed in the dendrites will enhance its pressure sensitivity and, by extension, influence *C* of the composite. In addition, Prasad et al. [34] have determined that *C* of BMGs increases with increasing temperature, provided the temperature does not exceed ~0.7 T_g. This trend of variations in *C* were attributed to the increasing pressure sensitivity of flow in the BMG. In contrast, *C* either remains the same, or decreases with increasing temperature in crystalline alloys [40], indicating that it exhibits negligible pressure sensitivity. Considering that BMGCs contain both phases, it is worth examining the trend in variations of its *C* with temperature.

With the motivation to address these aspects of *C* and pressure sensitivity, hardness tests and uniaxial compression tests were performed on two BMGCs, one containing non-transforming β-Ti dendrites and the other with transforming β-Ti dendrites, and a BMG at temperatures in the range of 0.48 -0.75 T_g. Both BMGCs are microstructurally similar in terms of the dendrite size, their volume fraction and morphology. Moreover, the composition of the BMGCs were chosen such that the volume fraction of the dendritic phase is ~50%, with the intention of facilitating equipartitioning of strain in both phases. Results indicate that *C* of the BMGC with transforming dendrites (BMGC-T) is higher than that of the other BMGC and the BMG, at the lowest temperature of testing. However, with increasing temperature, *C* of the former decreases, while that of the BMGC, with non-transforming dendrites (BMGC-NT), and the BMG, increases. To rationalize these experimental observations, the variations in the hardness of the individual phases and the yield strengths of the alloys with temperature were examined. Finally, the relative influence of the pressure sensitivities of flow in the constituents and the deformation mechanisms on the hardness and yield strength of the two BMGCs were discussed and compared with that of the BMG.

2. Materials and methods

2.1. Material and microstructural characterization

The ingots of a BMG, $Ti_{32}Zr_{30.1}Cu_9Co_{4.9}Be_{24}$ (at.%), and two BMGCs, $Ti_{44.8}Zr_{32.3}Cu_{5.7}Co_5Be_{12.2}$ (at.%) and $Ti_{46.6}Zr_{33.7}Cu_{5.9}Co_1Be_{12.8}$ (at.%), were prepared by arc-melting a mixture of Ti, Zr, Cu, Co, and Be, with a purity > 99.8%, in a Ti-gettered high purity argon atmosphere. All alloy ingots were re-melted four times to ensure chemical homogeneity and then cast in copper molds to fabricate Ø 8mm cylindrical rods. More processing details of these alloys can be found elsewhere [13,15,27,43]. Slices with a thickness of 1 mm were transversely cut from the as-cast rods using wire cut electrical discharge machining (EDM). They are ground and mechanically polished to a mirror-like finish for microstructural observations. A scanning electron microscope (FESEM, JEOL, JSM-7800F), in back scattered electron (BSE) mode, combined with Energy-dispersive X-ray spectroscopy (EDS) was utilized to determine the microstructure and composition of the alloys, respectively. EBSD (Thermo Scientific Apreo 2C, Oxford Symmetry S2) was employed to examine stress-induced martensitic transformation within crystalline dendrites. Additional small pieces, each weighing 10 mg, were sectioned from all the alloys rods to perform differential scanning calorimetry (DSC, Netzsch 404 F3 Pegasus), at a heating rate of 20 K/min. The glass transition temperature, T_g, of each alloy was estimated from their DSC scans. A Rigaku Ultima IV, X-Ray Diffractometer was used to perform X-ray diffraction (XRD) on the alloys.

2.2. Material nomenclature

For ease of reference, alloys are labelled according to their microstructural characteristics. Representative SEM images of the $Ti_{32}Zr_{30.1}Cu_9Co_{4.9}Be_{24}$, $Ti_{44.8}Zr_{32.3}Cu_{5.7}Co_5Be_{12.2}$ and $Ti_{46.6}Zr_{33.7}Cu_{5.9}Co_1Be_{12.8}$ alloys are shown in Fig. 1 (a), (b), and (c), respectively. While $Ti_{32}Zr_{30.1}Cu_9Co_{4.9}Be_{24}$ is featureless, $Ti_{44.8}Zr_{32.3}Cu_{5.7}Co_5Be_{12.2}$ and $Ti_{46.6}Zr_{33.7}Cu_{5.9}Co_1Be_{12.8}$ contain a dendritic phase embedded within the matrix. XRD scans obtained from the three alloys are shown in Fig. 1 (d). A diffused broad hump, with a peak at 2θ ~37°, is observed in the scan of $Ti_{32}Zr_{30.1}Cu_9Co_{4.9}Be_{24}$, which indicates that the alloy is fully amorphous and is hence referred to as BMG. In contrast, scans of both $Ti_{44.8}Zr_{32.3}Cu_{5.7}Co_5Be_{12.2}$ and $Ti_{46.6}Zr_{33.7}Cu_{5.9}Co_1Be_{12.8}$ contain diffraction peaks superimposed over a diffused broad hump, which correspond to a body centred cubic (bcc) phase and an amorphous matrix, respectively. On this basis, both alloys are referred to as BMGC. In addition, the nomenclature includes a reference to the tendency of the dendritic phase to undergo stress-induced martensitic transformation (further details on these will be provided later). The suffixes, 'T' and 'NT' are used for referring to the transforming and non-transforming nature of the dendrites, respectively. Therefore, $Ti_{44.8}Zr_{32.3}Cu_{5.7}Co_5Be_{12.2}$, which contains non-transforming dendrites and $Ti_{46.6}Zr_{33.7}Cu_{5.9}Co_{1}Be_{12.8}$, which contains transforming ones, will hitherto be referred to as BMGC-NT and BMGC-T, respectively.

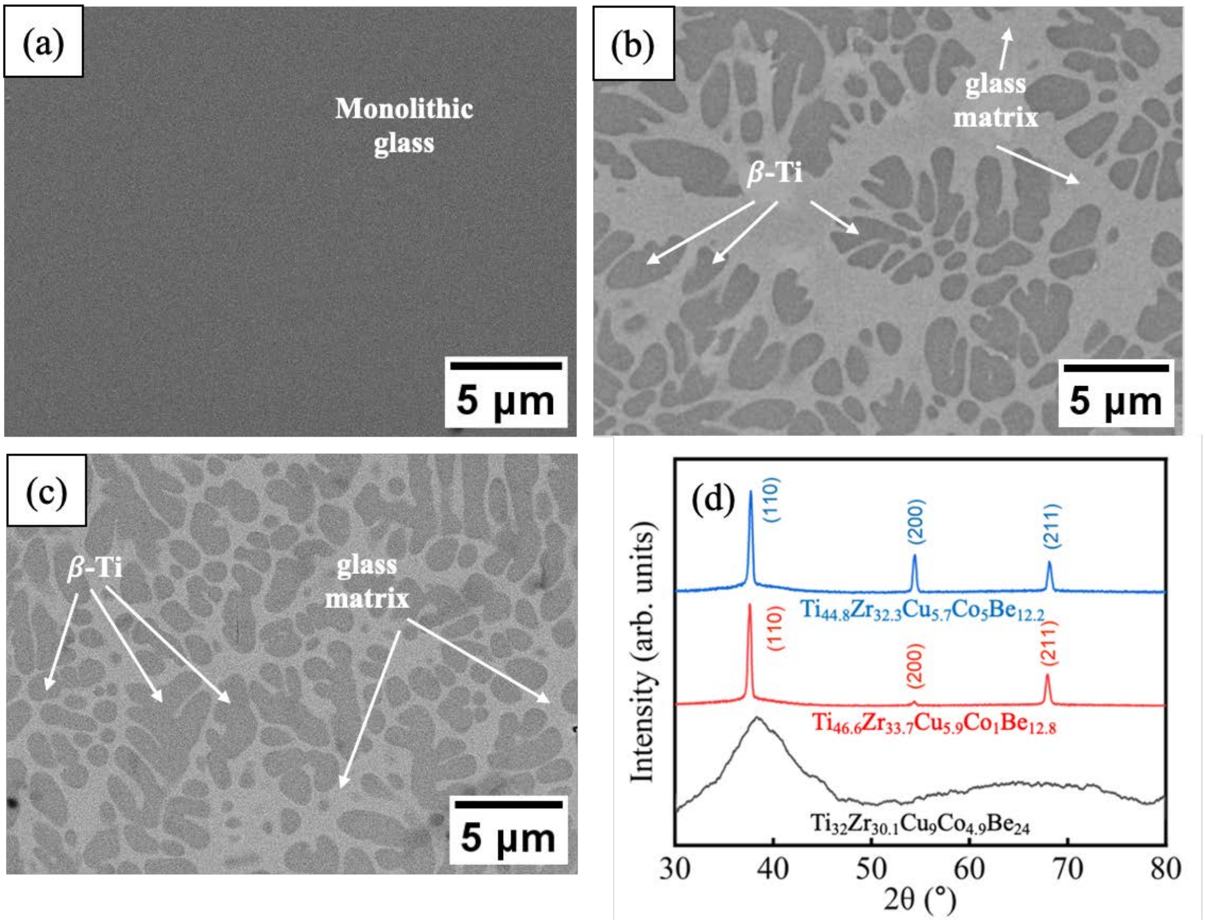

Fig. 1. Representative microstructures of (a) $Ti_{32}Zr_{30.1}Cu_{9}Co_{4.9}Be_{24}$ (BMG), (b) $Ti_{46.6}Zr_{33.7}Cu_{5.9}Co_{1}Be_{12.8}$ (BMGC-T) and (c) $Ti_{44.8}Zr_{32.3}Cu_{5.7}Co_{5}Be_{12.2}$ (BMGC-NT) and (d) their XRD scans.

2.3. Nanoindentation tests

From cylindrical rods of each alloy, 8 mm (diameter) × 3 mm (thickness) discs are extracted for performing nanoindentation tests to determine their hardness, *H*. Tests are performed using the Hysitron Triboindenter TI980, which is equipped with a Berkovich tip. A maximum load, P_{max}, of 5 N was applied at a loading rate of 250 mN/s (which corresponds to a nominal strain rate of 0.05/s), and a dwell time of 5 s are employed for all indentations. For the BMG and

BMGC-NT, tests were performed at temperatures of 290, 330, 390, and 450 K. For the BMGC-T, tests were performed at 300, 350, 415, and 480 K. These temperatures were specifically used as they correspond to 0.48, 0.55, 0.65, and 0.75 times T_g for the tested alloys. Note that T_g corresponds to the transition from the glassy state to the supercooled liquid regime for all BMGs (including the glass matrix in BMGCs), which makes it the ideal normalizing parameter for the temperature of testing, across the three compositions. To measure H of individual phases, a maximum load of 1 mN was applied at a loading rate of 50 μN/s (nominal strain rate of 0.05/s). Since significant pile-up occurs at the edges of all the indenter imprints, H of the composite and individual phases was estimated by dividing the maximum load applied by the projected area of the indents [36,42,46]. A minimum of 15 measurements were performed on each phase and the average of these values are reported. The projected areas of the indents were measured using the atomic force microscopy (AFM Flex Axiom, Nanosurf) and in-situ scanning probe microscopy (SPM) feature of the Triboindenter TI980.

For the high temperature nanoindentation experiments, it was ensured that each specimen was kept at the desired temperature for less than 10 minutes, which is much lesser than the corresponding α-relaxation time-scales of the amorphous matrices [47,48]. A fresh sample was employed for performing tests at each temperature to minimize the effects of structural relaxation.

2.4. Compression tests

Uniaxial compression tests were carried out on mirror polished specimens, having length of 5 mm and aspect ratio of 1.7, using a universal testing machine (UTM; Z030 TN Zwick/Roell). The tests were performed at a strain rate of 0.001 s^{-1} at temperatures corresponding to 0.48, 0.55, 0.65, and 0.75 times T_g for each alloy. Graphite lubricant was applied on the grooves to minimize the frictional stresses between the platens and the specimen. For high temperature testing, samples were heated at a rate of ≈20 K/min, and then held at the set temperatures for about 5 minutes. Temperature is monitored by a thermocouple and a small glass window on the front door of the furnace enabled real-time observation of the sample during the test. After testing, the specimen was allowed to cool to room temperature before extracting the fractured specimens. To ensure repeatability, a minimum of three tests were performed on each alloy and at each temperature.

3. Results

3.1. Microstructural characterization

Fig. S1 of the supplementary information (SI) displays the representative EDS maps of BMG, BMGC-T, and BMGC-NT. In both the BMGCs, Zr is evenly distributed in the dendrites and matrix. While the matrices of the two are lean in Co and Cu, their dendrites are commensurately rich with them. The differences in the contrast of the matrix and dendrites in Fig. 1 can be attributed to these compositional variations. One key difference in the compositions of the dendrites in BMGC-T and BMGC-NT is that the Co content in the former is significantly lesser than that in the latter. Regardless, they are referred to as the β-Ti phase since Ti is the major constituent in the dendrites. Table 1 lists the overall chemical compositions of the BMG and the two BMGCs, as well as the dendrites and matrices of the BMGCs. Their microstructural characteristics, such as volume fraction, V_d, size, δ, and interdendritic spacing, λ, are also listed. Note that both BMGC-NT and BMGC-T have similar microstructural parameters; both have V_d of ~50%, δ that ranges from 2.13 ±0.76 μm to 3.82 ±1.39 μm and λ that ranges from 0.95 ± 0.47 to 1.28 ± 0.98 μm.

Table 1: The compositions and abbreviated names of the investigated BMG and BMGCs. The measured volume fraction, V_d, the average size of secondary β-Ti dendritic arms, δ, and the EDS-determined compositions of both phases in the BMGCs are also listed.

Material	Chemical composition (wt%)		T_g (K)	V_d (%)	δ (μm)	λ (μm)
	Dendrite	Matrix				
BMG ($Ti_{32}Zr_{30.1}Cu_9Co_{4.9}Be_{24}$)	–	–	603	–	–	–
BMGC-NT ($Ti_{44.8}Zr_{32.3}Cu_{5.7}Co_5Be_{12.2}$)	$Ti_{60.1}Zr_{36.3}Cu_{2.1}Co_{1.5}$	$Ti_{32.02}Zr_{30.13}Cu_{9.01}Co_{4.84}Be_{24}$	608	49.19 ± 0.78	2.13 ± 0.76	1.28 ± 0.98
BMGC-T ($Ti_{46.6}Zr_{33.7}Cu_{5.9}Co_1Be_{12.8}$)	$Ti_{62.8}Zr_{34.3}Cu_{2.5}Co_{0.4}$	$Ti_{32.02}Zr_{30.13}Cu_{9.01}Co_{4.84}Be_{24}$	640	50.97 ± 0.96	3.82 ± 1.39	0.95 ± 0.47

The DSC traces of the BMG and two BMGCs are shown in Fig. 2. In all of them, an endothermic event above 560 K, corresponding to the glass transition, is followed by a supercooled liquid region. At even higher temperatures, one or two exothermic peaks are observed, which correspond to the occurrence of crystallization. The T_g of BMG, BMGC-NT, and BMGC-T are 603, 603, and 640 K, respectively. Just below T_g, an exothermic hump is also observed in all the DSC traces. The area under the exothermic humps corresponds to the enthalpy of relaxation, ΔH_{rel}, which corresponds to the energy difference between the 'as quenched' and fully relaxed state of the amorphous matrix. ΔH_{rel} provides a quantitative measure of the structural state of the glass matrix, i.e., a lower value suggests that the structure is more relaxed [4,15]. Additionally, an additional exothermic hump well below the T_g is observed in the DSC scans of BMGC-T and BMGC-NT, which corresponds to the partial transformation of β-Ti to ω-Ti [13,15,16]. The calculated values of ΔH_{rel} of the matrices of BMG, BMGC-NT and BMGC-T are 8.23, 5.12 and 6.75 J/g, respectively. From these, it was determined that the amorphous matrix of BMGC-NT is more structurally relaxed than that of BMGC-T and BMG.

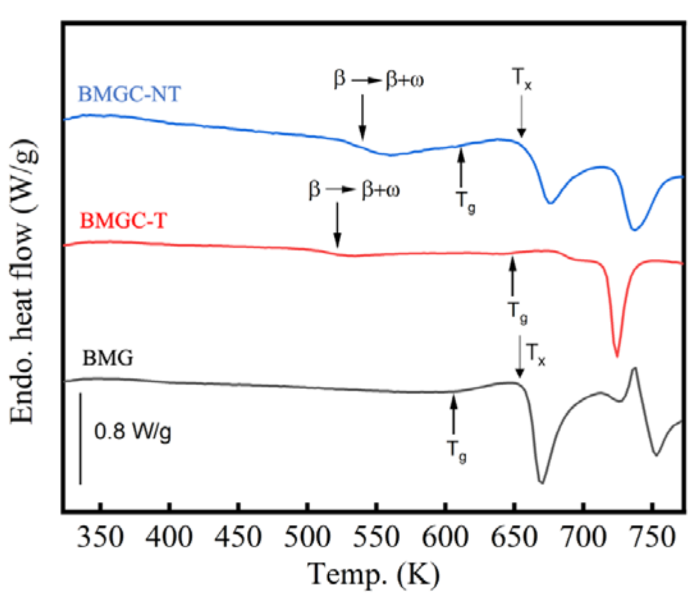

Fig. 2. DSC scans obtained from the BMG, BMGC-T and BMGC-NT.

3.2. Temperature dependence of mechanical properties

3.2.1. Variation of yield strength with temperature

Figs. 3 (a)-(c) show the representative engineering stress, σ, vs. engineering strain, ε, curves obtained at different temperatures of BMG, BMGC-T and BMGC-NT, respectively. The nature of the σ-ε curves for all three are similar irrespective of the temperature of testing. The linear elastic portion followed by a smooth transition to a non-linear portion after yield that corresponds to plastic deformation. The yield strengths, σ_y, of BMG and BMGC-NT at each temperature are estimated using the 0.2% offset method. It was noted that BMGC-T exhibits two-stage hardening behaviour at all temperatures. This is characterized by the presence of two non-linear segments in the σ-ε curve (see section S1 in SI). Zhu et al. [24] performed uniaxial tensile tests on this alloy and observed a similar two stage hardening behaviour referring to it as ‘double yielding’. In this event, determining σ_y of the material using the 0.2% offset method is inappropriate. Therefore, the method employed by Bhattacharjee et al. [49] for materials exhibiting two stage hardening, is employed for measuring σ_y from σ-ε curve of BMGC-T samples at different temperatures (see Fig. S2 for details).

The variations of σ_y as a function of test temperature are shown in Fig. 3 (d). At 0.48*T*g, BMG and BMGC-T have the highest and lowest σ_y of ~1.65 and ~0.93 GPa, respectively, whereas σ_y of BMGC-NT has an intermediate value of ~1.25 GPa. However, with increasing temperature, σ_y of both BMG and BMGC-NT decreases. For instance, at 0.48T_g, the σ_y of BMG and BMGC-NT are 1.65 and 1.25 GPa, respectively, whereas at 0.75T_g, they are 1.29 and 0.99 GPa, respectively. In contrast, σ_y of BMGC-T increases with temperature. In fact, at 0.75T_g, σ_y of BMGC-T is 0.11 GPa higher than that of BMGC-NT.

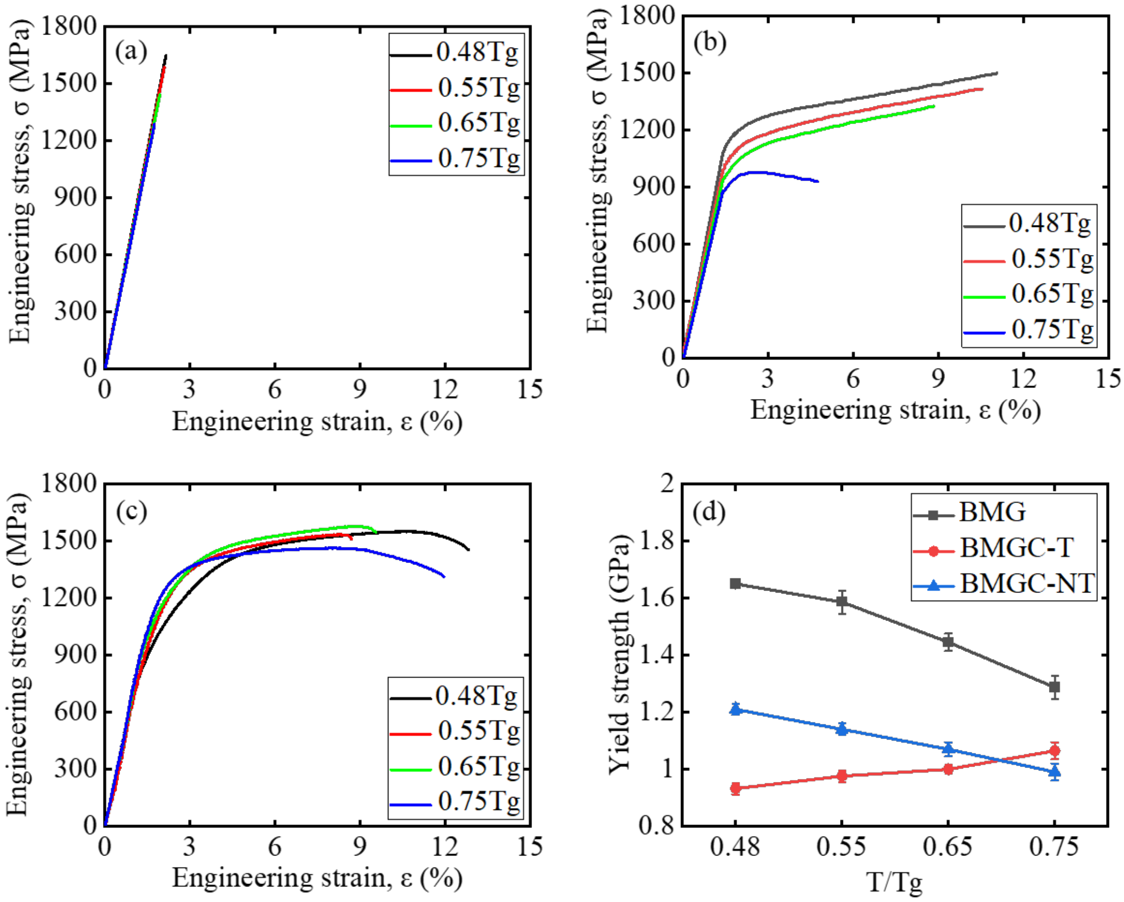

Fig. 3. Uniaxial compression stress-strain responses of the (a) BMG, (b) BMGC-NT, (c) BMGC-T and (d) variations of σ_y of the alloys as function of temperature.

To understand the post yield plasticity, the strain hardening exponent, *n*, is obtained by fitting the portion of the flow curves between YS and UTS with the power-law, $\sigma^T = K(\varepsilon^T)^n$, where K is a constant, σ^T is the true stress, and ε^T is the true strain. *n* has a fixed value of ~ 0.19 for BMGC-NT, in the temperature range of 0.48 T_g to 0.65 T_g but reduces to ~ 0.16 at 0.75 T_g. Similarly, for BMGC-T, n ~ 0.45, at all temperatures, except at 0.75 T_g, where n ~ 0.37. The variations in the strain hardening rate, dσ/dε, of both BMGCs, with ε^T, at different temperatures is shown in Fig. S3. Broadly, dσ/dε decreases to zero, from an initially high value, with increasing ε^T for both BMGCs at all temperatures. However, while dσ/dε decreases gradually with increasing ε^T for both BMGCs at 0.48 T_g, it becomes progressively steeper with increasing temperature. This indicates that strain hardening at 0.48 T_g extends to large strains but as the temperature is increased, it saturates at significantly smaller plastic strains.

3.2.2. Hardness of BMG, BMGCs and its constituents

3.2.2.1. Macrohardness and constraint factor variations with temperature

Figs. 4 (a)-(c) display the images of indentation impressions on BMG, BMGC-NT and BMGC-T. The length of each side of the impressions on them are ~43.2, ~46, and ~44.2 μm, respectively. Since δ and λ of the two BMGCs are an order of magnitude smaller than the sides of the impressions (see Fig. 1), the indentation impression encompasses a significant area of both dendrites and matrix. It is therefore expected that these tests provide the overall hardness, *H*, of the two BMGCs.

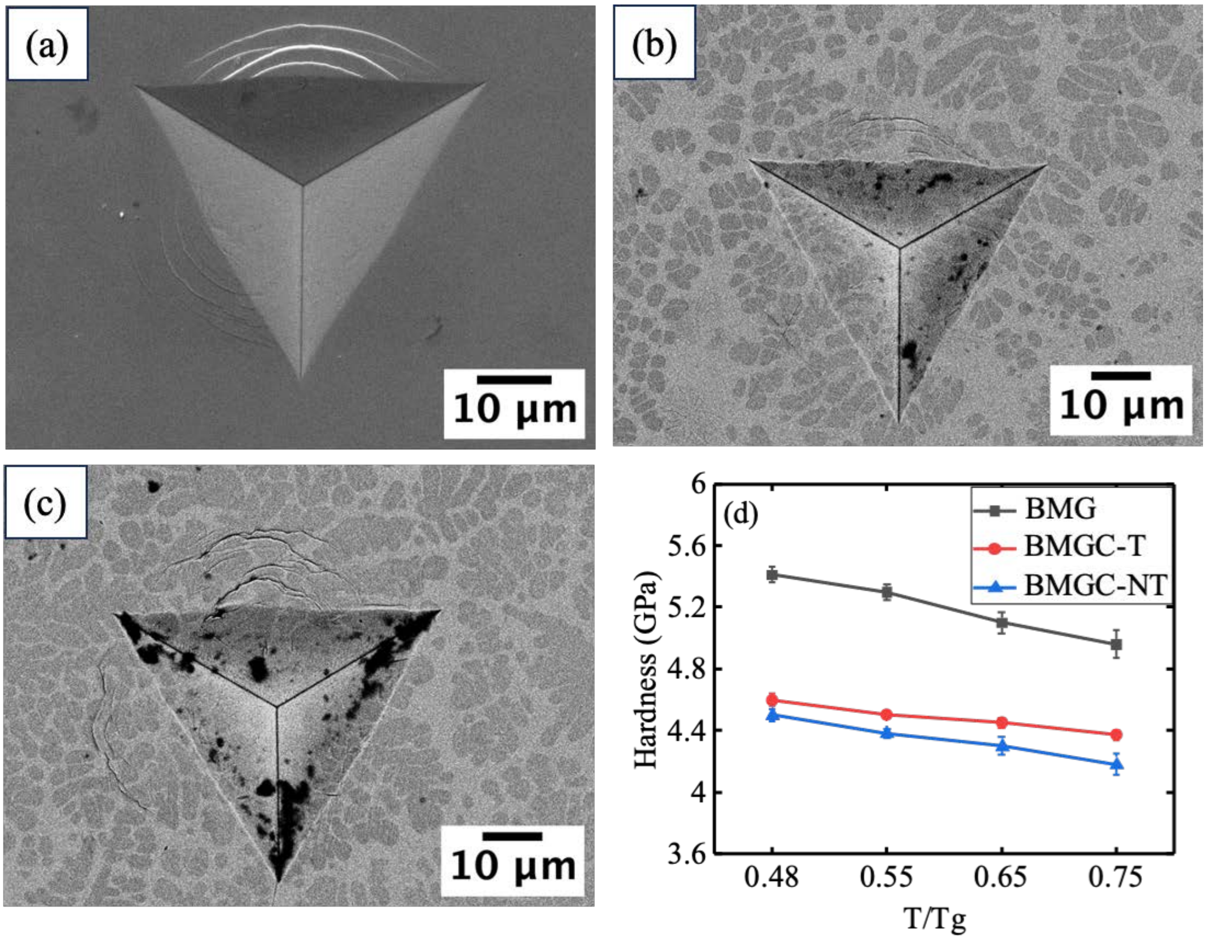

Fig. 4. Images of the indenter imprints at 0.48*T*g in (a) BMG, (b) BMGC-NT and (c) BMGC-T. (d) Variations in *H* of the three alloys plotted as a function of temperature.

The variations in *H* of the three alloys is plotted as a function of temperature in Fig. 4 (d). At 0.48 T_g, BMG has the highest *H* of ~5.41 GPa whereas that of BMGC-NT is ~4.5 GPa, which is the lowest. BMGC-T has an intermediate *H* of ~4.6 GPa. With increasing temperature, *H* of all the alloys decrease. However, the magnitude of drop in *H* is 14% in the case of BMG and only 7% in the case of both BMGC-NT and BMGC-T, when the temperature is increased from 0.48 to 0.75T_g.

In Figs. 5 (a) and (b), the EBSD phase maps of the area around the indenter impressions in BMGC-T that were tested at 0.48 and 0.75T_g, respectively, are shown. For comparison, the EBSD phase maps of regions around the indenter impressions in BMGC-NT tested at 0.48 and

$0.75T_g$ are shown in Figs. 5 (c) and (d), respectively. Similarly, the phase maps of the indenter impressions of both composites tested at other temperatures are shown in Fig. S4. The regions with dark contrast correspond to the amorphous matrix whereas the green and red coloured regions represent the β-Ti phase and α”-Ti phase, respectively. From these, it is evident that several β-Ti dendrites close to the edges of the indent impressions appear to have transformed to α”-Ti in BMGC-T at all the testing temperatures. In contrast, in BMGC-NT, β-Ti dendrites near the indenter edges do not undergo α”-Ti transformation at any temperature.

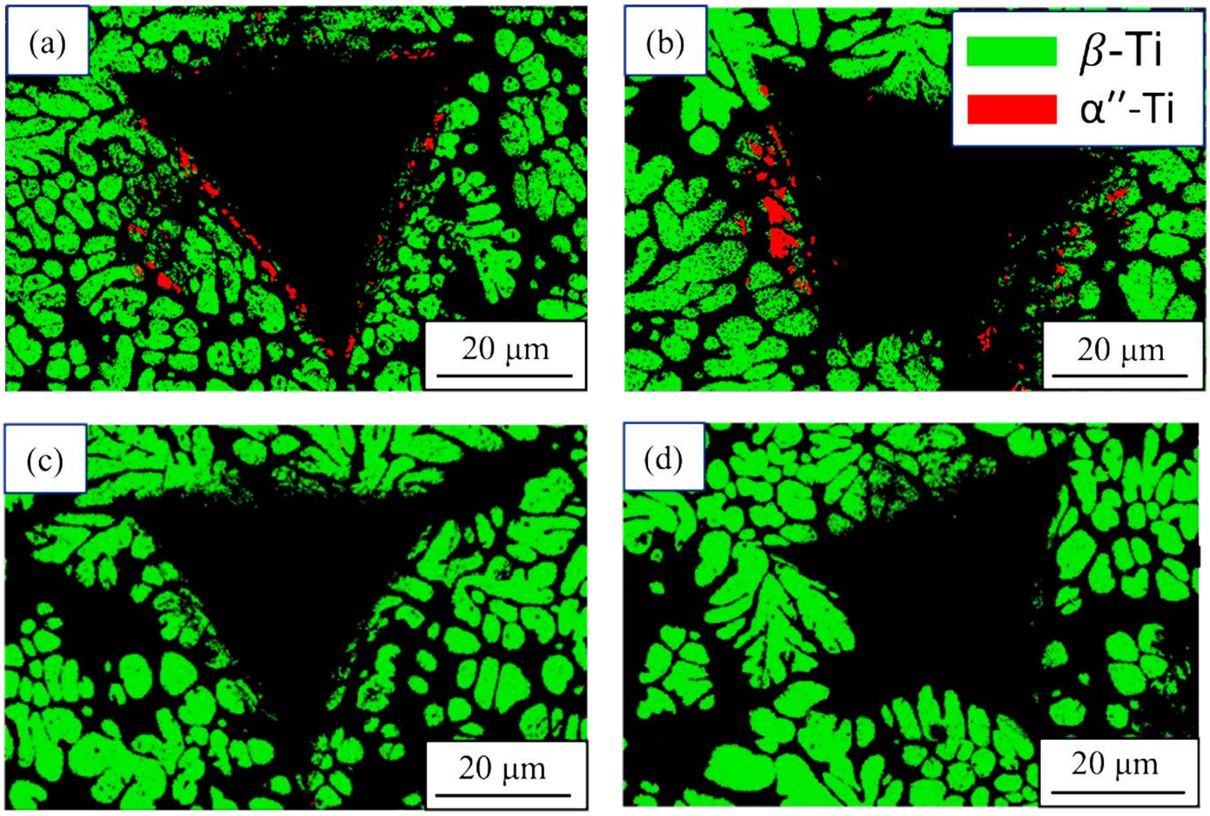

Fig. 5. EBSD phase maps for BMGC-T at (a) $0.48T_g$, (b) $0.75T_g$ and for BMGC-NT at (c) $0.48T_g$ and (d) $0.75T_g$.

To obtain further insights into the plastic constraint enforced by the matrix surrounding the indented material, we examine the constraint factor, C ($=H/\sigma_y$) of the alloys. The variations in C of BMG, BMGC-NT and BMGC-T as a function of temperature are displayed in Fig. 6. At $0.48T_g$, BMG and BMGC-T have the lowest and highest C of ~ 3.28 ± 0.04 and 4.93 ± 0.15, respectively. At the same temperature, BMGC-NT has an intermediate *C* of ~ 3.72 ± 0.09. With an increase in temperature, *C* of BMG monotonically increases, and attains a value of 3.85 at 0.75 T_g. Similarly, *C* of BMGC-NT also increases from 3.72 to 4.22 in the same temperature range. However, *C* of BMGC-T dramatically decreases with temperature. In fact, the decrease is so precipitous that *C* of BMGC-T is similar to that of BMGC-NT and BMG at 0.75T_g.

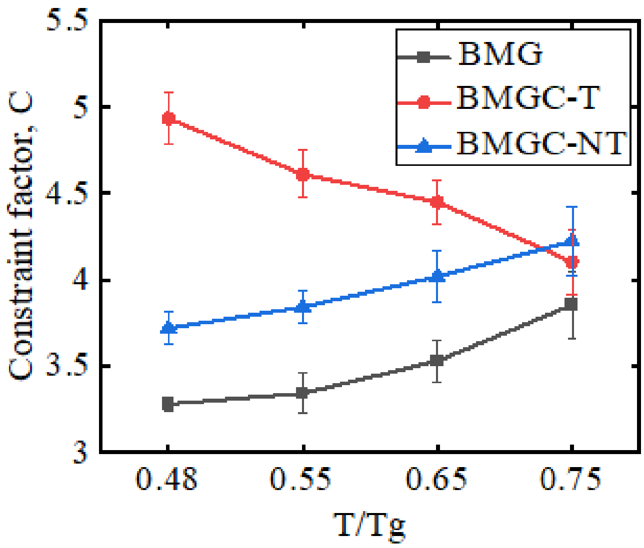

Fig. 6. Constraint factor variations for the three alloys as a function of temperature.

Overall, BMG is harder than the two BMGCs at all temperatures. However, while the hardness of BMG decreases significantly with temperature, that of BMGC-T and BMGC-NT is broadly invariant, within a reasonable error band. BMGC-T offers the highest constraint to plastic flow at 0.48T_g followed by BMGC-NT and BMG. While this constraint in BMG and BMGC-NT increases with increasing temperature, that of BMGC-T decreases considerably.

3.2.2.2. Surface deformation around indent imprints

As can be seen in Fig. 4, macroscopic plasticity in BMGs and the matrices of BMGCs manifest in the form of shear bands. Therefore, to further assess the extent of plastic deformation in the three alloys during indentation, the number of shear bands in the regions around the indenter impressions on all alloys, shown in Figs. 4 and S5 are counted. An illustration of the counting method is shown in Fig. S6. The variations in the number of shear bands, N_s, around the indenter impressions of all alloys are plotted as a function of temperature in Fig. 7 (a). At 0.48T_g, BMG has the highest N_s of 10 ± 1, whereas that of BMGC-NT is 5 ± 1 which is the lowest amongst the three alloys. BMGC-T has an intermediate N_s of 8 ± 1 at the same temperature. These differences in N_s of the three alloys are attributed to the relative free volume contents in them. Note that a greater free volume content, which is directly scales with ΔH_{rel} of the amorphous phase [4], enhances the propensity of shear band formation. From Fig. 2, it was observed that ΔH_{rel} of the BMG and BMGC-NT are the highest and lowest, respectively, whereas that of BMGC-T has an intermediate value, which is similar to the trend observed in N_s. With increase in temperature, there is a steady decrease in N_s in all the three alloys. While N_s linearly decreased with the temperature in the case of BMGC-T and BMGC-NT, the decrease in N_s of BMG is much more precipitous. In fact, at 0.75T_g, N_s of BMGC-NT and BMGC-T are 2 and 5, whereas that of BMG is approximately similar to that of BMGC-T.

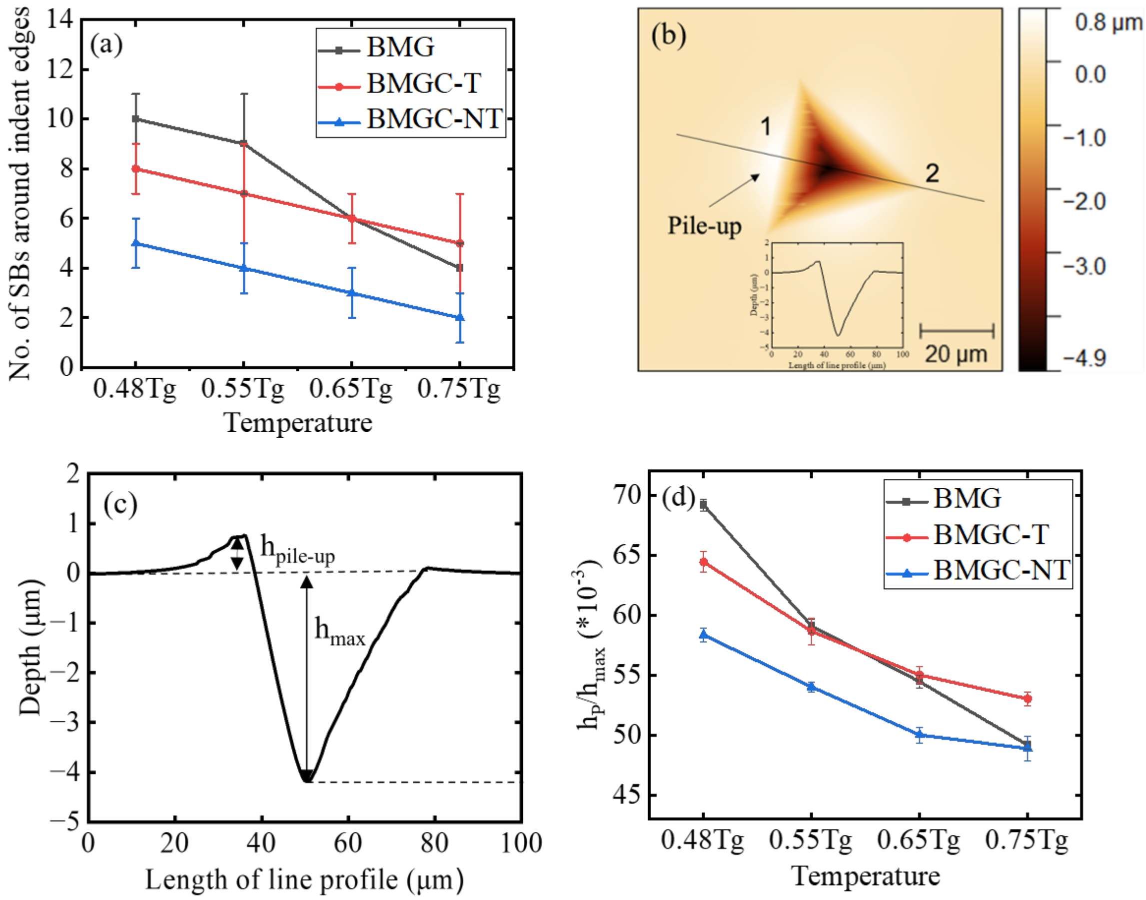

Fig. 7: (a) Variations in number of shear bands (SBs) around indent edges with temperature, (b) SPM image of residual imprint and its line profile, (c) line profile of nanoindentation imprint in BMG at 0.48 T_g and (d) variations in the degree of pile-up with temperature.

To further understand the characteristics of the shear band mediated plastic zones around the indenter impressions, the extent of pile-up around them are investigated. A representative SPM image of the residual indenter imprint and its line profile are shown in Fig. 7 (b). From the line scan of these images the pile up height, h_p, and total indentation depth, h_{max}, (see Fig. 7 (c) for reference), is measured. Then, for each alloy, normalized pile-up height, h_p/h_{max}, is calculated. Its variations as a function of temperature are shown in Fig. 7 (d). At $0.48T_g$, h_p/h_{max} of BMG, BMGC-NT and BMGC-T are 0.069, 0.058 and 0.064, respectively. This implies that the extent of pile-up in BMGCs is lower than that in BMGs. With an increase in temperature, h_p/h_{max} of all the three alloys decreases monotonically. The decrease is however more dramatic in the case of BMG as its h_p/h_{max} is the lowest and same as that of BMGC-NT at $0.75T_g$. In summary, the number of shear bands around the indenter impression in all alloys decreases with temperature. It was also observed that number of shear bands and the extent of pile-up is higher in BMG than in both BMGCs, below $0.55\ T_g$. However, at higher temperatures, the number of shear bands in BMGs is similar to that in BMGC-T and its extent of pile-up is similar to that in BMGC-NT.

3.2.2.3. Hardness variations of individual phases in BMGCs with temperature

The variations of H of the dendrites and matrices in BMGC-NT and BMGC-T, as a function of temperature, are shown in Fig. 8. The subscripts, *d* and *m*, refer to the dendrite and matrix phases, respectively. Some representative SPM images of the indents on each alloy and its constituent phases are shown in Fig. S7. At all temperatures, in both BMGCs, the matrices are harder than the dendrites. For instance, at $0.48T_g$, H_d and H_m are 2.44 ± 0.06 4.66 ± 0.13 GPa, respectively, in BMGC-NT. Their respective values are and 2.8 ± 0.07 and 4.7 ± 0.14 GPa in BMGC-T. Previous reports confirm that the dendritic phase is significantly softer than the amorphous matrix in the β-Ti reinforced BMGCs [13,42]. With increasing temperature, H_m in both the composites decreases whereas H_d remains invariant. The minimal reduction in H_d with increasing temperature is because the reference temperature for the amorphous matrix is T_g whereas it is T_m for the crystalline phase. Note the latter ranges between 1,554 - 1,649°C for β-Ti. This implies that the current range of temperatures is much below $0.4T_m$, which is the temperature above which there is significant softening of the phase occurs. As a consequent, significant changes in H_d are not expected. At $0.75T_g$, H_m of BMGC-NT and BMGC-T are 4.36 ± 0.18 and 4.49 ± 0.19 GPa, respectively, both of which are lesser than the respective values at $0.48T_g$.

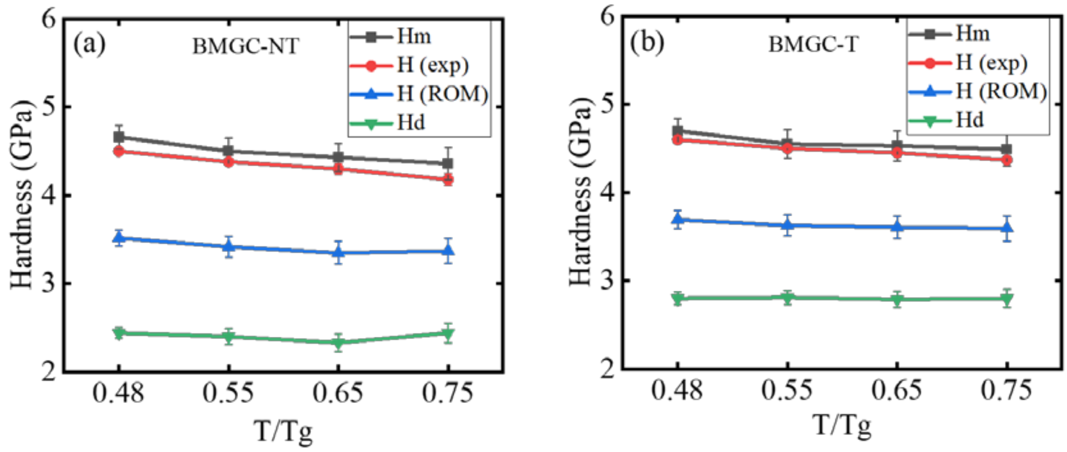

Fig. 8. Variations of experimental and estimated values of hardness of (a) BMGC-NT and (b) BMGC-T, as a function of temperature.

To understand the relative contributions of the two phases to the overall H of the composites, we use the rule of mixtures (ROM) as a reference, which is as follows,

$$H\ (ROM) = V_d H_d + V_m H_m \tag{1}$$

where V_m and V_d are the volume fractions of the matrix and dendrite, respectively. From eq. (1), the calculated values of H (ROM), at all temperatures, for both BMGC-T and BMGC-NT are determined and plotted in Fig. 8. For reference, the experimentally determined values of H of the corresponding BMGCs are also included in the same plots (see Fig. 4 (d)) (denoted by 'exp'). Note that, at all temperatures, the calculated values of H are considerably lower than the experimentally determined ones. Instead, the latter matches closely with the corresponding H_m. While some previous studies [42] have also reported the similarity of H_m and H, they were measured only at room temperature. The present results confirm that the H_m controls H of both the BMGCs in the entire temperature range of 0.48 – 0.75 T_g.

4. Discussion

4.1. Effect of temperature on deformation and pressure sensitivity of BMG and BMGCs

The unit carriers of plasticity in BMGs are shear transformation zones (STZs), whose shear strain induced activation and linking up leads to the formation of shear bands. This implies that the onset of yielding in BMGs is governed by the stress required to activate STZs, which in turn depends on temperature and to some extent on the alloy composition [42,50–61]. Typically, at higher temperatures, thermal input aids shear induced activation of STZs, which then occurs at lower stresses [9,52,54,55,60–63]. For this reason, σ_y of BMGs is expected to decrease with increasing temperature, which was indeed observed in this study (see Fig. 3 (a)). Although both BMGCs considered in this study have an amorphous matrix, their σ_y is not solely governed by the amorphous matrices. At the outset, while σ_y of the amorphous matrices in both BMGCs could not be directly measured, it is expected to match well with that of the BMG examined in this study, given that their compositions are similar. However, the considerably lower σ_y of the BMGC-NT and BMGC-T, compared to that of the BMG (see Fig. 3 (d)), indicates that the softer reinforcing β-Ti phase influences yielding of the composite significantly. In fact, several studies have suggested that σ_y of the BMGC is controlled by the yielding of the β-Ti dendrites, to the extent that σ_y is modelled well by a ROM approximation of the yield strengths of the two phases [42,64]. On this basis, it can be asserted that at the lowest temperature of testing ($0.48T_g$), BMGC-NT, which has higher σ_y than BMGC-T, has the stronger dendrites of the two. Note that plasticity in β-Ti dendrites of BMGC-NT is mediated by dislocation slip. However, previous studies have shown that in the dendrites of BMGC-T, yielding initiates when the applied stress transforms the β-Ti phase to the orthorhombic martensitic phase, α”-Ti [13]. It has been determined that the stress required for initiating this stress-induced martensitic transformation (SIMT) is lower than that required to initiate slip [13,24,27,43]. This explains the lower σ_y of BMGC-T compared to that of BMGC-NT at $0.48T_g$ (see Table 1). With increasing temperature, the activation of dislocation slip in β-Ti dendrites of BMGC-NT becomes progressively easier. In combination with the reduction in the stress to activate shear induced activation of STZs in the amorphous matrix, σ_y of BMGC-NT decreases. Alternately, previous studies have shown that the effect of temperature on critical stress for SIMT is well described by the following Clausius-Claperyon relationship [65]:

$$\frac{d\sigma_{cr}}{dT} = -\frac{\Delta S}{\varepsilon} \quad (2)$$

where σ_{cr} is the critical stress for SIMT, T is the temperature, ΔS is the variation in entropy and ε is the applied strain. ΔS is defined as [66],

$$\Delta S = NK_B \ln\left(\frac{V_f}{V_i}\right) \quad (3)$$

where N is Avogadro number, K_B is Boltzmann constant, V_i is the volume of initial phase, i.e., β-phase (body-centered cubic) and V_f is the volume of final phase formed after transformation, i.e., α''-phase (face centered orthorhombic). V_i and V_f are determined from [67–70],

$$V_i = \frac{a_\beta^3}{2} \quad (4)$$

$$V_f = \frac{a_{\alpha''} b_{\alpha''} c_{\alpha''}}{4} \quad (5)$$

where a_β is the lattice parameter of β phase, $a_{\alpha''}$, $b_{\alpha''}$ and $c_{\alpha''}$ are lattice parameters of the α''-phase. The lattice parameters of β-Ti and α''-Ti, in this study, are a_β ~0.332 nm, $a_{\alpha''}$ ~0.300 nm, $b_{\alpha''}$ ~0.503 nm and $c_{\alpha''}$ ~0.468 nm [67–70]. Substituting these values in equations (2), (3) and (4), the calculated change in volume ΔV, and, ΔS, are ~-0.0007 nm^3 and ~-0.324 J/(mol-K), respectively. From eq. (2), it is seen that since ΔS is negative, $\frac{d\sigma_{cr}}{dT}$ is always positive, which implies that σ_{cr} increases with increasing temperature [32,65]. This implies that a higher stress is required to trigger SIMT in β-Ti dendrites at elevated temperatures, which in turn, increases σ_y of the BMGC [32]. In fact, the increase in σ_y of BMGC-T with increasing temperature suggests that the increase in σ_{cr} of its dendrites more than compensates for the accompanied decrease in the strength of the amorphous matrix (see Fig. 3 (c)).

The decrease in the n of both BMGC-NT and BMGC-T at 0.75 T_g compared to that at 0.48 T_g is attributed to enhanced recovery at higher temperatures, which mitigates strain hardening. There is an additional influence of the increase in σ_{cr} with increasing temperature in BMGC-T. Note that the dendrites in BMGC-T, undergo the β-Ti to α"-Ti transformation, which locally reorients the lattice of the β-Ti and enhances dislocation interactions. This leads to significant work hardening of the dendrite as well as that of the BMGC-T. It is then reasonable to infer that a higher extent of β-Ti to α"-Ti transformations would lead to greater strain hardening of BMGC-T. It must then be recalled that BMGC-T will have lower volume fraction of β-Ti transformed to α"-Ti at 0.75 T_g, owing to the higher σ_{cr} required to facilitate this martensitic transformation. Therefore, the combined effect of enhanced recovery and higher σ_{cr} at higher temperatures reduces the strain hardening exponent of the BMGC-T at 0.75 T_g.

Interestingly, it was observed that H, which is also a measure of the resistance to plastic flow, of both BMGC-T and BMGC-NT, is influenced largely by the hardness of the amorphous matrices (H_m) in them (see Fig. 8 (b)). As mentioned earlier in the introduction, during the hardness test, the continuum surrounding the indented material acts as a constraint, which enhances the flow resistance of the material. In addition, Narasimhan [38], Patnaik et al. [39] and Prasad et al. [34] have reported that amorphous solids such as BMGs exhibit pressure sensitivity in flow stress, unlike crystalline materials. Since there is significant hydrostatic compression below the indenter, BMGs experience an even higher flow resistance during indentation than crystalline alloys. The relatively higher C of BMGs, as is reported in this study and several other prior studies [33–37,42], is an outcome of this effect. Extending this argument, Narayan et al. [42] suggested that the greater plastic constraint offered by the amorphous matrix, compared to that of the crystalline dendrites, is the reason the former has an overbearing influence on the *H* of BMGCs. They also concluded that the lesser influence of dendrites on *H* of the BMGC vis-à-vis the significant influence on σ_y is responsible for the enhancement in its *C*, over and above that of BMGs. The elevated values of *C* of BMGC-T and BMGC-NT, at $0.48T_g$, is attributed to the same reason. Amongst the two, BMGC-T has a significantly higher *C* owing to its lower σ_y, which in turn, is the outcome of the relatively lower stresses required for initiating SIMT in its dendrites.

With increasing temperature, besides a reduction in the stress required to trigger the STZs, there is enhanced diffusion assisted activation (DAA) of STZs as well in BMGs [9]. DAA, which is analogous to the β-relaxation process, involves short-range or medium-range diffusion of atoms present in the STZ clusters under an applied stress. Its occurrence enhances the homogeneous plastic deformation of BMGs and mitigates strain localization. Therefore, with increasing degree of DAA of STZs, the number of shear bands formed during plastic deformation decreases [9,52,61]. It and the degree of pile up (measured as h_p/h_{max}) around indenter impressions (see Figs. 7 (a, d)), of all the three alloys examined in this work, with increasing temperature, are indicative of enhanced DAA of STZs in the amorphous phase. At the outset, the stress required for DAA of STZs is lower than that required for activation of STZs with purely mechanical loads. However, the former is significantly more pressure sensitive than the latter. This is because DAA STZ requires long range atomic motion, which, in turn, requires significant dilation of the STZ cluster. In comparison, shear assisted STZ activation requires much lesser dilation of the cluster as it only involves short range motion of atoms. It is then evident that the presence of a positive hydrostatic pressure, such as that below the indenter, will restrict atomic motion more in the case of the DAA STZs. Therefore, to facilitate plastic flow at higher temperatures, where diffusion assisted transformation of STZs is the dominant deformation mechanism, a higher stress is required. Owing to this effect, at higher temperatures, the flow stress of the material under the indenter is significantly higher compared to that in the material tested in uniaxial compression, where the plastic constraint is considerably lower. This leads to an increase in *C* with increasing temperature, as was observed in our study for the BMG (see Fig. 6). A similar increase in *C* of BMGs with increasing temperature was observed in several prior studies as well [34,36,37]. These studies have also rationalized the increase in *C* by alluding to the increase in the pressure sensitivity of the dilatational strain, with increasing temperature. The enhanced pressure sensitivity of the flow stress of the amorphous phase with increasing temperature also implies that the H_c of both the BMGCs at higher temperatures will still be controlled by that of their amorphous matrices, which was indeed observed in Fig. 8. Given that the increasing pressure sensitivity of the amorphous phase with increasing temperature enhances *H* of the BMGC-NT and that there is a concomitant decrease in its σ_y, the increase in its *C* with increasing temperature is justified. Alternately, since the relative increase in the σ_y of BMGC-T, owing to the increase in the σ_c of the β-Ti dendrite, is considerably higher than the increase in its *H* with increasing temperature, its *C* decreases with increasing temperature. It is also worth noting that since *H* is mainly governed by H_m, and not H_d, the variations in the strain hardening behaviour of the BMGCs, which is governed by the changes in the deformation mechanisms in the dendrites, do not influence their *H* or *C*.

4.2. Other considerations

For BMGs, the hardness test is expected to provide additional insights, compared to uniaxial tests, in terms of the influence of pressure sensitivity on its flow stress at different temperatures [33]. In fact, Keryvin et al. [36] found a direct correlation between *C* and the pressure sensitivity index of BMGs. However, the preceding discussions indicate that while the hardness test on in situ β-Ti reinforced BMGCs provides an exclusive understanding of the pressure sensitivity of its amorphous matrix, it is unable to capture the plastic deformation characteristics of the dendrites. In contrast, the uniaxial compression tests, which are only partially constrained, can provide more information on the deformation mechanisms in both phases.

It is also evident that the minimal influence of the hardness of β-Ti (H_d) on H of the BMGCs, is an outcome of the negligible pressure sensitivity on its flow stress even at elevated temperatures. A previous study on the temperature variations of constraint factor in Ti-6Al-4V, a crystalline alloy, supports this observation and in fact, concludes that the pressure sensitivity of the flow stress in Ti-6Al-4V decreases with increasing temperature [40]. This also aligns well with the notion that the appropriate yield criterion for alloys that deform via dislocation slip are typically formulated by excluding normal or hydrostatic components of the Cauchy stress tensor. However, the minimal pressure sensitivity of the transforming β-Ti dendrites in BMGC-T is surprising as the SIMT to α"-Ti, which occurs at all the temperatures considered (see Fig. 5 and Fig. S4), involves change in volume. This volume change should, in principle, lead to the development of hydrostatic strains in the transforming β-Ti dendrites, and lead to increased pressure sensitivity of flow stress as well as C. One possible reason for the absence of pressure sensitivity in flow stress of these dendrites is that the volume change during SIMT of β-Ti to α"-Ti is negative (ΔV ~-0.0007 nm^3). Since this will manifest as negative volumetric strain in the dendrites, it will not be affected by the positive hydrostatic pressure under the indenter. Therefore, pressure sensitivity in flow stress of crystalline dendrites in BMGCs should only manifest when the volume change during their SIMT is positive. A systematic investigation of the pressure sensitivity of flow stress in such a scenario is a topic for future studies. Next, it is imperative to consider the influence of the ω-Ti phase on the hardness of the BMGCs. Zhang et al. [13] noted earlier that both transforming and non-transforming β-Ti dendrites contain ω-Ti phase in the as cast state of the BMGCs. Since the ω-Ti phase is a hard and brittle phase, it is likely to influence the hardness of the β-Ti dendrite. However, since the hardness of the BMGC is determined by that of the matrices and not by that of dendrites, the presence of ω-Ti in the dendrites is not expected to influence the hardness or constraint factors of the BMGCs at any temperature.

Before concluding, we note that *C* can be a qualitative parameter in gauging the processability of a material in the context of processing methods such as die forging, rolling and equi-channel angular processing, where the loading conditions are inherently constrained. Based on the results of the present study, since *C* of BMGC-NT and BMG is lowest at low or ambient temperatures but increases with increasing temperature, their processability at lower temperatures is considerably higher than that at high temperatures. The converse of this is true in BMGC-T, appears to exhibit better processability at higher temperatures. In Fig. S8, *C* of several crystalline and amorphous materials at different temperatures is shown. Note that *C* of crystalline materials generally decreases with increasing temperature. Therefore, in terms of preferred conditions for processing, BMGC-T is similar to crystalline materials, which also exhibit better processability at higher temperatures.

5. Conclusions

Instrumented indentation tests and uniaxial compression tests were performed on a BMG and two BMGCs, one with stress induced phase transforming dendrites and the other with non-transforming dendrites, at four temperatures below their T_g. Experimental results reveal that the constraint factor of the two BMGCs is 13-50% higher than that of the BMG at the lowest temperature of testing. Moreover, with increasing temperature, the constraint factor increases in the case of BMG and the BMGC with non-transforming dendrites but decreases in the one with transforming dendrites. While the variations in constraint factor of BMGs with temperature has been justified previously as the outcome of the increase in the pressure sensitivity of plastic flow at higher temperatures, that of BMGCs is rationalized on the basis of the flow stress variations of the individual phases in the hardness and uniaxial compression test. It was noted that while the yield strength of the BMGCs is predicted well by a weighted average of the strengths of the two phases, their hardness corresponds to that of their amorphous matrices. The latter is the outcome of the overbearing influence of the pressure sensitivity of the amorphous matrix on the plastically constrained material under the indenter. This disparity in the contributions of the phases to the plastic flow of the BMGC leads to the observed variations in the constraint factor. Finally, the pressure insensitive flow of the transforming dendrites is attributed to the net decrease in volume reduction during its stress induced transformation.

Acknowledgements

PS and RLN acknowledge the financial support provided by the Science and Engineering Research Board, Department of Science & Technology (No. SRG/2020/000095), and the Prime Minister Fellowship (PMRF) (No. PMRF/2021/1401226). BL and LZ acknowledge the support by the National Natural Science Foundation of China (52171164), the National Key Laboratory of Science and Technology on Materials under Shock and Impact (WDZC2022-13), and the Youth Innovation Promotion Association CAS (2021188). PS and RLN would also like to acknowledge the Central Research Facility, IIT Delhi for the access of FESEM-EDS. The authors further acknowledge the help provided by Prof. N.M. Anoop Krishnan, Prof. Nitya Nand Gosvami, Sourav Sahoo and Shweta R. Keshri (IIT Delhi) in DSC and AFM experiments.

References:

[1] C. Schuh, T. Hufnagel, U. Ramamurty, Mechanical behavior of amorphous alloys, Acta Mater. 55 (2007) 4067–4109. https://doi.org/10.1016/j.actamat.2007.01.052.

[2] A.L. Greer, Y.Q. Cheng, E. Ma, Shear bands in metallic glasses, Mater. Sci. Eng. R Rep. 74 (2013) 71–132. https://doi.org/10.1016/j.mser.2013.04.001.

[3] U. Ramamurty, S. Jana, Y. Kawamura, K. Chattopadhyay, Hardness and plastic deformation in a bulk metallic glass, Acta Mater. 53 (2005) 705–717. https://doi.org/10.1016/j.actamat.2004.10.023.

[4] P. Murali, U. Ramamurty, Embrittlement of a bulk metallic glass due to sub- annealing, Acta Mater. 53 (2005) 1467–1478. https://doi.org/10.1016/j.actamat.2004.11.040.

[5] Z.F. Zhang, J. Eckert, L. Schultz, Difference in compressive and tensile fracture mechanisms of Zr59Cu20Al10Ni8Ti3 bulk metallic glass, Acta Mater. 51 (2003) 1167–1179. https://doi.org/10.1016/S1359-6454(02)00521-9.

[6] A. Jain, Y. Prabhu, D. Gunderov, R.L. Narayan, P. Saini, S. Vincent, P. Sudha, A.D. Bagde, J. Bhatt, Structural characterization, biocorrosion and in-vitro investigation on Zr62Cu22Al10Fe5Dy1 metallic glass for bio-implant applications, J. Non-Cryst. Solids. 598 (2022) 121928. https://doi.org/10.1016/j.jnoncrysol.2022.121928.

[7] T. Mukai, T.G. Nieh, Y. Kawamura, A. Inoue, K. Higashi, Dynamic response of a Pd40Ni40P20 bulk metallic glass in tension, Scr. Mater. 46 (2002) 43–47. https://doi.org/10.1016/S1359-6462(01)01193-9.

[8] R.L. Narayan, L. Tian, D. Zhang, M. Dao, Z.-W. Shan, K.J. Hsia, Effects of notches on the deformation behavior of submicron sized metallic glasses: Insights from in situ experiments, Acta Mater. 154 (2018) 172–181. https://doi.org/10.1016/j.actamat.2018.05.041.

[9] P.S. Singh, R.L. Narayan, I. Sen, D.C. Hofmann, U. Ramamurty, Effect of strain rate and temperature on the plastic deformation behaviour of a bulk metallic glass composite, Mater. Sci. Eng. A. 534 (2012) 476–484. https://doi.org/10.1016/j.msea.2011.11.096.

[10] S. Gouripriya, P. Tandaiya, Three-Dimensional Unit Cell Study of a Porous Bulk Metallic Glass Under Various Stress States, J. Appl. Mech. 86 (2019) 061010. https://doi.org/10.1115/1.4042995.

[11] J.W. Qiao, A.C. Sun, E.W. Huang, Y. Zhang, P.K. Liaw, C.P. Chuang, Tensile deformation micromechanisms for bulk metallic glass matrix composites: From work-hardening to softening, Acta Mater. 59 (2011) 4126–4137. https://doi.org/10.1016/j.actamat.2011.03.036.

[12] R.L. Narayan, P.S. Singh, D.C. Hofmann, N. Hutchinson, K.M. Flores, U. Ramamurty, On the microstructure–tensile property correlations in bulk metallic glass matrix

composites with crystalline dendrites, Acta Mater. 60 (2012) 5089–5100. https://doi.org/10.1016/j.actamat.2012.06.032.
[13] L. Zhang, R.L. Narayan, H.M. Fu, U. Ramamurty, W.R. Li, Y.D. Li, H.F. Zhang, Tuning the microstructure and metastability of β-Ti for simultaneous enhancement of strength and ductility of Ti-based bulk metallic glass composites, Acta Mater. 168 (2019) 24–36. https://doi.org/10.1016/j.actamat.2019.02.002.
[14] L. Zhang, Z. Zhu, H. Fu, H. Li, H. Zhang, Improving plasticity and work-hardening capability of β-type bulk metallic glass composites by destabilizing β phases, Mater. Sci. Eng. A. 689 (2017) 404–410. https://doi.org/10.1016/j.msea.2017.02.070.
[15] D. Rajpoot, R.L. Narayan, L. Zhang, P. Kumar, H. Zhang, P. Tandaiya, U. Ramamurty, Shear fracture in bulk metallic glass composites, Acta Mater. 213 (2021) 116963. https://doi.org/10.1016/j.actamat.2021.116963.
[16] D. Rajpoot, R.L. Narayan, L. Zhang, P. Kumar, H. Zhang, P. Tandaiya, U. Ramamurty, Fracture toughness of a rejuvenated β-Ti reinforced bulk metallic glass matrix composite, J. Mater. Sci. Technol. 106 (2022) 225–235. https://doi.org/10.1016/j.jmst.2021.09.001.
[17] Y. Chen, C. Tang, J.-Z. Jiang, Bulk metallic glass composites containing B2 phase, Prog. Mater. Sci. 121 (2021) 100799. https://doi.org/10.1016/j.pmatsci.2021.100799.
[18] Y. Ren, T. Yan, Z. Huang, Q. Zhou, K. Hua, X. Li, Y. Du, Q. Jia, L. Zhang, H. Zhang, H. Wang, Cryogenic wear behaviors of a metastable Ti-based bulk metallic glass composite, J. Mater. Sci. Technol. 134 (2023) 33–41. https://doi.org/10.1016/j.jmst.2022.06.027.
[19] L. Zhang, T. Yan, D. Şopu, Y. Wu, B. Jiang, K. Du, H. Zhang, J. Eckert, Shear-band blunting governs superior mechanical properties of shape memory metallic glass composites, Acta Mater. 241 (2022) 118422. https://doi.org/10.1016/j.actamat.2022.118422.
[20] K.K. Song, S. Pauly, Y. Zhang, R. Li, S. Gorantla, N. Narayanan, U. Kühn, T. Gemming, J. Eckert, Triple yielding and deformation mechanisms in metastable Cu47.5Zr47.5Al5 composites, Acta Mater. 60 (2012) 6000–6012. https://doi.org/10.1016/j.actamat.2012.07.015.
[21] D.C. Hofmann, Bulk Metallic Glasses and Their Composites: A Brief History of Diverging Fields, J. Mater. 2013 (2013) 1–8. https://doi.org/10.1155/2013/517904.
[22] T. Yan, L. Zhang, R.L. Narayan, J. Pang, Y. Wu, H. Fu, H. Li, U. Ramamurty, H. Zhang, Effects of Al addition and cryogenic cyclic treatment on impact toughness of phase-transformable Ti-based bulk metallic glass composites, J. Mater. Sci. Technol. 140 (2023) 210–220. https://doi.org/10.1016/j.jmst.2022.09.008.

[23] J. Zhou, H. Wu, Y. Wu, W. Song, R. Chen, C. Tan, G. Xie, D. Cao, H. Wang, X. Liu, S. Jiang, X. Wang, Z. Lu, Enhancing dynamic mechanical properties of bulk metallic glass composites via deformation-induced martensitic transformation, Scr. Mater. 186 (2020) 346–351. https://doi.org/10.1016/j.scriptamat.2020.05.012.

[24] R.T. Zhu, J.L. Yuan, Z. Wang, X.H. Shi, H.J. Yang, J.W. Qiao, "Double-yielding" behavior and progressive β → α → twins transformation in a Ti-based metallic glass matrix composite, Scr. Mater. 218 (2022) 114838. https://doi.org/10.1016/j.scriptamat.2022.114838.

[25] X. Fu, G. Wang, Y. Wu, W. Song, C.H. Shek, Y. Zhang, J. Shen, R.O. Ritchie, Compressive ductility and fracture resistance in CuZr-based shape-memory metallic-glass composites, Int. J. Plast. 128 (2020) 102687. https://doi.org/10.1016/j.ijplas.2020.102687.

[26] H. Zhai, H. Wang, F. Liu, A strategy for designing bulk metallic glass composites with excellent work-hardening and large tensile ductility, J. Alloys Compd. 685 (2016) 322–330. https://doi.org/10.1016/j.jallcom.2016.05.290.

[27] L. Zhang, R.L. Narayan, B.A. Sun, T.Y. Yan, U. Ramamurty, J. Eckert, H.F. Zhang, Cooperative Shear in Bulk Metallic Glass Composites Containing Metastable β -Ti Dendrites, Phys. Rev. Lett. 125 (2020) 055501. https://doi.org/10.1103/PhysRevLett.125.055501.

[28] D.C. Hofmann, J.-Y. Suh, A. Wiest, G. Duan, M.-L. Lind, M.D. Demetriou, W.L. Johnson, Designing metallic glass matrix composites with high toughness and tensile ductility, Nature. 451 (2008) 1085–1089. https://doi.org/10.1038/nature06598.

[29] C.C. Hays, C.P. Kim, W.L. Johnson, Microstructure Controlled Shear Band Pattern Formation and Enhanced Plasticity of Bulk Metallic Glasses Containing *in situ* Formed Ductile Phase Dendrite Dispersions, Phys. Rev. Lett. 84 (2000) 2901–2904. https://doi.org/10.1103/PhysRevLett.84.2901.

[30] X.Z. Ma, D.Q. Ma, H. Xu, H.Y. Zhang, M.Z. Ma, X.Y. Zhang, R.P. Liu, Enhancing the compressive and tensile properties of Ti-based glassy matrix composites with Nb addition, J. Non-Cryst. Solids. 463 (2017) 56–63. https://doi.org/10.1016/j.jnoncrysol.2017.02.025.

[31] L. Zhang, H. Fu, H. Li, Z. Zhu, H. Zhang, W. Li, Y. Li, H. Zhang, Developing β-type bulk metallic glass composites from Ti/Zr-based bulk metallic glasses by an iteration method, J. Alloys Compd. 740 (2018) 639–646. https://doi.org/10.1016/j.jallcom.2018.01.005.

[32] J.L. Yuan, R.T. Zhu, P.D. Han, Z. Wang, Martensite transformation govern serration deformation of a metastable metallic glass matrix composite, Intermetallics. 156 (2023) 107855. https://doi.org/10.1016/j.intermet.2023.107855.

[33] A. Dubach, K. Eswar Prasad, R. Raghavan, J.F. Löffler, J. Michler, U. Ramamurty, Free-volume dependent pressure sensitivity of Zr-based bulk metallic glass, J. Mater. Res. 24 (2009) 2697–2704. https://doi.org/10.1557/jmr.2009.0304.

[34] K. Eswar Prasad, R. Raghavan, U. Ramamurty, Temperature dependence of pressure sensitivity in a metallic glass, Scr. Mater. 57 (2007) 121–124. https://doi.org/10.1016/j.scriptamat.2007.03.033.

[35] S.S. Hirmukhe, K.E. Prasad, I. Singh, Investigation of pressure sensitive plastic flow in nanoglasses from finite element simulations, Scr. Mater. 180 (2020) 45–50. https://doi.org/10.1016/j.scriptamat.2020.01.022.

[36] V. Keryvin, K. Eswar Prasad, Y. Gueguen, J.-C. Sanglebœuf, U. Ramamurty, Temperature dependence of mechanical properties and pressure sensitivity in metallic glasses below glass transition, Philos. Mag. 88 (2008) 1773–1790. https://doi.org/10.1080/14786430802286971.

[37] K.E. Prasad, V. Keryvin, U. Ramamurty, Pressure sensitive flow and constraint factor in amorphous materials below glass transition, J. Mater. Res. 24 (2009) 890–897. https://doi.org/10.1557/jmr.2009.0113.

[38] R. Narasimhan, Analysis of indentation of pressure sensitive plastic solids using the expanding cavity model, Mech. Mater. 36 (2004) 633–645. https://doi.org/10.1016/S0167-6636(03)00075-9.

[39] M.N.M. Patnaik, R. Narasimhan, U. Ramamurty, Spherical indentation response of metallic glasses, Acta Mater. 52 (2004) 3335–3345. https://doi.org/10.1016/j.actamat.2004.03.028.

[40] A. Kumaraswamy, B. Venkataraman, Effect of temperature on constraint factor of Ti–6Al–4V under static indentation conditions, Scr. Mater. 54 (2006) 493–498. https://doi.org/10.1016/j.scriptamat.2005.06.020.

[41] T. Rouxel, J. Jang, U. Ramamurty, Indentation of glasses, Prog. Mater. Sci. 121 (2021) 100834. https://doi.org/10.1016/j.pmatsci.2021.100834.

[42] R.L. Narayan, K. Boopathy, I. Sen, D.C. Hofmann, U. Ramamurty, On the hardness and elastic modulus of bulk metallic glass matrix composites, Scr. Mater. 63 (2010) 768–771. https://doi.org/10.1016/j.scriptamat.2010.06.010.

[43] L. Zhang, S. Chen, H.M. Fu, H. Li, Z.W. Zhu, H.W. Zhang, Z.K. Li, A.M. Wang, H.F. Zhang, Tailoring modulus and hardness of in-situ formed β-Ti in bulk metallic glass composites by precipitation of isothermal ω-Ti, Mater. Des. 133 (2017) 82–90. https://doi.org/10.1016/j.matdes.2017.07.062.

[44] A. Rastogi, R. Sarkar, S. Neelakantan, Transitions among martensitic phases during continuous deformation in metastable β Ti-10V-2Fe-3Al alloy, J. Alloys Compd. 964 (2023) 171320. https://doi.org/10.1016/j.jallcom.2023.171320.

[45] A. Rastogi, S. Neelakantan, Enhanced thermo-mechanical processing through stress-induced martensitic transformation and its effect on grain refinement in metastable β titanium alloys, Scr. Mater. 226 (2023) 115222. https://doi.org/10.1016/j.scriptamat.2022.115222.

[46] A. Bhattacharyya, G. Singh, K. Eswar Prasad, R. Narasimhan, U. Ramamurty, On the strain rate sensitivity of plastic flow in metallic glasses, Mater. Sci. Eng. A. 625 (2015) 245–251. https://doi.org/10.1016/j.msea.2014.12.004.

[47] P. Saini, R.L. Narayan, On simultaneous enhancement in local yield strength and plasticity of short-term annealed bulk metallic glasses, J. Alloys Compd. 898 (2022) 162960. https://doi.org/10.1016/j.jallcom.2021.162960.

[48] W.H. Wang, Dynamic relaxations and relaxation-property relationships in metallic glasses, Prog. Mater. Sci. 106 (2019) 100561. https://doi.org/10.1016/j.pmatsci.2019.03.006.

[49] A. Bhattacharjee, V.K. Varma, S.V. Kamat, A.K. Gogia, S. Bhargava, Influence of β grain size on tensile behavior and ductile fracture toughness of titanium alloy Ti-10V-2Fe-3Al, Metall. Mater. Trans. A. 37 (2006) 1423–1433. https://doi.org/10.1007/s11661-006-0087-x.

[50] A.S. Argon, Plastic deformation in metallic glasses, Acta Metall. 27 (1979) 47–58. https://doi.org/10.1016/0001-6160(79)90055-5.

[51] V. Keryvin, Indentation of bulk metallic glasses: Relationships between shear bands observed around the prints and hardness, Acta Mater. 55 (2007) 2565–2578. https://doi.org/10.1016/j.actamat.2006.12.005.

[52] U. Ramamurty, M.L. Lee, J. Basu, Y. Li, Embrittlement of a bulk metallic glass due to low-temperature annealing, Scr. Mater. 47 (2002) 107–111. https://doi.org/10.1016/S1359-6462(02)00102-1.

[53] B.-G. Yoo, K.-W. Park, J.-C. Lee, U. Ramamurty, J. Jang, Role of free volume in strain softening of as-cast and annealed bulk metallic glass, J. Mater. Res. 24 (2009) 1405–1416. https://doi.org/10.1557/jmr.2009.0167.

[54] J. Lu, G. Ravichandran, W.L. Johnson, Deformation behavior of the Zr41.2Ti13.8Cu12.5Ni10Be22.5 bulk metallic glass over a wide range of strain-rates and temperatures, Acta Mater. 51 (2003) 3429–3443. https://doi.org/10.1016/S1359-6454(03)00164-2.

[55] C.A. Schuh, A.C. Lund, T.G. Nieh, New regime of homogeneous flow in the deformation map of metallic glasses: elevated temperature nanoindentation experiments and mechanistic modeling, Acta Mater. 52 (2004) 5879–5891. https://doi.org/10.1016/j.actamat.2004.09.005.

[56] R.L. Narayan, D. Raut, U. Ramamurty, A quantitative connection between shear band mediated plasticity and fracture initiation toughness of metallic glasses, Acta Mater. 150 (2018) 69–77. https://doi.org/10.1016/j.actamat.2018.03.011.

[57] R.L. Narayan, P. Tandaiya, R. Narasimhan, U. Ramamurty, Wallner lines, crack velocity and mechanisms of crack nucleation and growth in a brittle bulk metallic glass, Acta Mater. 80 (2014) 407–420. https://doi.org/10.1016/j.actamat.2014.07.024.

[58] R.L. Narayan, P. Tandaiya, G.R. Garrett, M.D. Demetriou, U. Ramamurty, On the variability in fracture toughness of ‘ductile’ bulk metallic glasses, Scr. Mater. 102 (2015) 75–78. https://doi.org/10.1016/j.scriptamat.2015.02.017.

[59] R.L. Narayan, P. Tandaiya, G.R. Garrett, M.D. Demetriou, U. Ramamurty, On the variability in fracture toughness of ‘ductile’ bulk metallic glasses, Scr. Mater. 102 (2015) 75–78. https://doi.org/10.1016/j.scriptamat.2015.02.017.

[60] T. Yan, L. Zhang, R.L. Narayan, J. Pang, Y. Wu, H. Fu, H. Li, H. Zhang, U. Ramamurty, Temperature-dependence of impact toughness of bulk metallic glass composites containing phase transformable β-Ti crystals, Acta Mater. 229 (2022) 117827. https://doi.org/10.1016/j.actamat.2022.117827.

[61] C. Wang, Q.P. Cao, X.D. Wang, D.X. Zhang, U. Ramamurty, R.L. Narayan, J.-Z. Jiang, Intermediate Temperature Brittleness in Metallic Glasses, Adv. Mater. 29 (2017) 1605537. https://doi.org/10.1002/adma.201605537.

[62] K. Eswar Prasad, U. Ramamurty, Effect of temperature on the plastic zone size and the shear band density in a bulk metallic glass, Mater. Sci. Eng. A. 535 (2012) 48–52. https://doi.org/10.1016/j.msea.2011.12.040.

[63] W.L. Johnson, K. Samwer, A Universal Criterion for Plastic Yielding of Metallic Glasses with a (T / T g) 2 / 3 Temperature Dependence, Phys. Rev. Lett. 95 (2005) 195501. https://doi.org/10.1103/PhysRevLett.95.195501.

[64] P. Gargarella, S. Pauly, M. Samadi Khoshkhoo, U. Kühn, J. Eckert, Phase formation and mechanical properties of Ti–Cu–Ni–Zr bulk metallic glass composites, Acta Mater. 65 (2014) 259–269. https://doi.org/10.1016/j.actamat.2013.10.068.

[65] J.P. Oliveira, R.M. Miranda, F.M. Braz Fernandes, Welding and Joining of NiTi Shape Memory Alloys: A Review, Prog. Mater. Sci. 88 (2017) 412–466. https://doi.org/10.1016/j.pmatsci.2017.04.008.

[66] D.R. Gaskell, D.E. Laughlin, Introduction to the thermodynamics of materials, Sixth edition, CRC Press, Taylor & Francis Group, CRC Press is an imprint of Taylor & Francis Group, an informa business, Boca Raton ; New York, 2018.

[67] X. Ji, I. Gutierrez-Urrutia, S. Emura, T. Liu, T. Hara, X. Min, D. Ping, K. Tsuchiya, Twinning behavior of orthorhombic-α” martensite in a Ti-7.5Mo alloy, Sci. Technol. Adv. Mater. 20 (2019) 401–411. https://doi.org/10.1080/14686996.2019.1600201.

[68] O.N. Senkov, B.C. Chakoumakos, J.J. Jonas, F.H. Froes, Effect of temperature and hydrogen concentration on the lattice parameter of beta titanium, Mater. Res. Bull. 36 (2001) 1431–1440. https://doi.org/10.1016/S0025-5408(01)00604-3.

[69] G. Han, X. Lu, Q. Xia, B. Lei, Y. Yan, C.J. Shang, Face-centered-cubic titanium - A new crystal structure of Ti in a Ti-8Mo-6Fe alloy, J. Alloys Compd. 748 (2018) 943–952. https://doi.org/10.1016/j.jallcom.2018.03.218.

[70] Y. Mantani, Y. Takemoto, M. Hida, A. Sakakibara, M. Tajima, Phase Transformation of α" Martensite Structure by Aging in Ti-8 mass%Mo Alloy, Mater. Trans. 45 (2004) 1629–1634. https://doi.org/10.2320/matertrans.45.1629.